Shock Wave and High Pressure Phenomena

Isabelle Sochet *Editor*

Blast Effects

Physical Properties of Shock Waves

Springer

Chapter 9
Small-Scale Blast Wave Experiments by Means of an Exploding Wire

Oren Sadot, Omri Ram, Eliram Nof, Eytan Kochavi, and Gabi Ben-Dor

9.1 Introduction

Understanding how blast waves interact with structures has become increasingly important over the past decades, especially in light of the increased threats of terror attacks. Blast–structure interactions depend on two processes: the dynamic loads imposed by the explosion and the structural response to these loads. The time scales of these two processes differ markedly, with that of blast propagation in the structure being significantly shorter than that of the response of the structure to the blast due to its large mass. In most cases, the difference between these two time scales justifies neglecting the effect of the motion of the structure on the propagation of the blast wave in the structure. Details concerning the structural response to the load can be found in Smith and Hetherington (1994).

In this chapter, we introduce a unique experimental tool that enables investigating the blast wave imposed load on a structure using different types of diagnostics systems.

Some studies on the dynamic loads associated with explosions are full-scale experiments, but such resource-intensive tests usually have inherent, obvious difficulties (Needham 2010; Dewey et al. 1977). Although numerous measuring techniques, including those based on high-speed photography, have been developed over the past few decades to measure the effects of blast waves on structures, their applicability is limited due to the sheer destructiveness of large-scale explosions. In fact, it is virtually impossible to monitor blast wave propagation and dynamic gas effects in full-scale urban scenario experiments using high-speed photography (Needham 2010; Dewey 2001). Instead, the data gleaned from full-scale urban

O. Sadot • O. Ram • E. Nof • E. Kochavi • G. Ben-Dor (✉)
Protective Technologies R&D Center, Faculty of Engineering Sciences, Ben-Gurion University of the Negev, Beer Sheva, Israel
e-mail: bendorg@bgu.ac.il

I. Sochet (ed.), *Blast Effects*, Shock Wave and High Pressure Phenomena,
https://doi.org/10.1007/978-3-319-70831-7_9

scenarios are limited to measurements from a small number of pressure transducers positioned in key locations inside the structures. But such data can help only in partially understanding blast wave flow patterns and propagation of blast waves inside the structures.

A widely used alternative technique to investigate the effects of an explosive event on structures exploits small-scale tests under laboratory conditions. Under controlled conditions, small-scale explosions can be easily created using chemical explosives such as silver-azide (Kleine et al. 2005; Hargather and Settles 2007). Such experiments utilize small charges that typically range from a few milligrams for a laboratory test (Kleine and Takayama 2004; Kleine et al. 2005; Hargather and Settles 2007; Cheval et al. 2010) to a few kilograms for a scaled-down field test (Neuberger et al. 2007). A variety of diagnostic methods, including pressure transducers and strain gauges placed in the vicinity of the explosion and on the tested structures (Reichenbach and Neuwald 2000) and optical diagnostic systems, can be used to measure the dynamic flow field and the structure response. Pressure transducers and strain gauges record the time history of the load developed by the explosion and the structural response to the load, while optical systems, such as schlieren or shadowgraph techniques, are used to monitor the blast wave propagation (Kleine and Takayama 2004; Hargather and Settles 2007; Reichenbach and Neuwald 2000; Settles 2001). The advantages of such small-scale experiments include their affordability (Kleine and Takayama 2004; Kleine et al. 2005) and the ease with which a large number of experiments can be safely conducted to verify and validate results obtained from numerical simulations. The validated results, in turn, can provide a better understanding of how wave propagation, flow pattern, and loads behave in actual explosions. Indeed, it has been shown that despite the obvious differences between the properties of small vs. large explosive charges, relatively good predictions can be made based on the information acquired in small-scale experiments combined with various scaling laws (Needham 2010; Dewey 2001; Hargather and Settles 2007).

One of the most comprehensive collections of experiments to study internal and external explosions in small-scale scenarios was published by Reichenbach and Neuwald (2000). In their examples, gram-scale explosive charges were used to study blast effects on buildings, stairways, tunnels, and other structures found in urban scenarios. Pressure transducers were used to measure the pressures produced by the explosions and shadowgraph or schlieren photography was used to monitor blast wave propagation in and around the structures. Likewise, the experiments of Smith et al. (1992) with small-scale internal and external explosions showed that the results can be used to obtain blast loading data in complex structures, such as tunnels and rooms. For example, they showed that a relatively good assessment of peak overpressure can be obtained using the well-known Crantz-Hopkinson scaling laws.

Small-scale blast experiments have been used to calibrate and validate numerical hydro-codes used to study a wide range of problems related to blast waves. Jiang et al. (1998) studied the micro-blast wave generated by a near instantaneous release of energy from a pulsed Nd:glass laser focused on a point several tens of microns in

diameter. Blast wave visualization by double-exposure holographic interferometry and numerical simulation showed that a spherical micro-blast wave is a valid tool for simulating the blast waves created in large-scale explosions. Rose and Smith (2002) studied the dependence of the positive and negative phase impulses of blast waves from explosive detonations on the geometric features of city streets (i.e., tall buildings on both sides of a street). Their small-scale experiments (1/40th scale), designed to model a 1000-kg TNT spherical explosive charge exploded at street level, were performed with 11.09 g DEMEX 100 type explosive, and their results were used to validate numerical stimulations (the three-dimensional blast simulation code "Air3d" was used). Zyskowski et al. (2004) used small-scale experiments together with numerical simulations to assess the effects of an accidental explosion of a confined hydrogen-air gas mixture cloud on nearby structures. They created a confined explosion by electrically igniting a hemispherical soap bubble filled with a mixture of hydrogen and oxygen and situated in a closed box. Reflected pressure histories on the box walls, measured at different distances from the explosion, were used to validate a numerical solution obtained using the AUTODYN commercial solver. The authors found better correlations for normal than for non-normal reflection areas and that the pressure measurements from the simulations were lower than those in the experiments.

Establishing our experimental design on the essence of the small-scale experiment, we developed an experimental tool to investigate the dynamic loads that are imposed on a structure by internal and external blast waves. We created small-scale explosions using the exploding wire approach, in which an applied high current pulse causes the abrupt evaporation of a thin metal conductor. Popular since the 1920s, this approach has been used mostly to study the electrical and physical phenomena associated with the behavior of the wire (Chase and Moore 1959). Nowadays, exploding wires are used to study the effects of high currents on, among other phenomena, conductors and the plasma state of matter. The strong blast wave that accompanies the exploding wire phenomenon has also been investigated by Bennet (1959), Buntzen (1962), and Higashino et al. (1991). Those studies used capacitor banks and fast, high current switches to evaporate the thin conductive wire and create the blast wave in an earth, a gas (air), or a liquid (water) medium. To monitor the blast propagation and pressure history, a high-speed, schlieren-based photography system and pressure transducers were used. To compare the experimental results to the numerical ones, the exploding wires were modeled in the simulations as high density, high temperature columns of air modeled as an ideal gas. Good agreement was found between the numerical calculations and the flow fields produced by the exploding wires (Higashino et al. 1991).

Based on the above studies and being aware of the potential of the exploding wire system for blast wave research, we built a similar system and developed the corresponding research methodology. The newly built system and its complementary numerical model enabled us to deepen our understanding of the complex blast–structure interaction phenomenon, predict blast flow behavior, and evaluate quantitatively the reliability of the numerical code.

The present chapter is organized as follows: the experimental system and the calibration process are first described, after which we demonstrate the effectiveness of the research methodology, present two test cases demonstrating the capabilities of the exploding wire facility to investigate the interaction of small-scale cylindrical and spherical blast waves with structures.

9.2 Experimental Setup

9.2.1 Exploding Wires

When a short, high-current pulse passes through a thin conducting wire, the wire undergoes a rapid Joule heating and evaporates. The current is created by discharging high voltage from a capacitor through the thin wire. Two basic circuits, the charging and discharging circuits, are connected to the capacitor, which is charged by a high-voltage power supply. The discharge circuit is connected to the capacitor through a fast-opening high-voltage switch whose closure connects the capacitor to the wire. This action permits the stored charge to flow through the thin wire causing a very high current pulse. The wire then undergoes a very fast Joule heating, which causes it to liquefy and vaporize with virtually no change in its volume. This leads to the creation of a very hot and dense vaporized metal column that starts to expand rapidly. The rapid expansion of the hot vaporized metal column drives a strong blast wave. A detailed explanation of this phenomenon can be found in Reithel et al. (1962).

The amount of charge stored in the capacitor is determined by the charging voltage, which is set before the experiment. If the energy is too low the wire exhibits "fuse"-like behavior that will not produce a blast wave. On the other hand, too much energy will produce non-repeatable results, and some electric energy will remain in the capacitor. Under correct working conditions, the exploding wires produce repeatable blast waves. The two energy limits must thus be found for each wire configuration. Exploding wires, by their nature, produce cylindrical blast waves, but as will be shown subsequently, we successfully extended the use of the exploding wire phenomenon to generate spherical explosions that drive spherical blast waves, which more closely resemble the spherical explosions generated by high explosive charges. In our system, spherical explosions were obtained by tying a knot in the wire (whose ends were held between the two electrodes (Fig. 9.1)) that was then exploded as discussed above. The wire was isolated to prevent an electrical short circuit. Thus, the small volume explosion produced by our system formed a perfectly spherical blast wave.

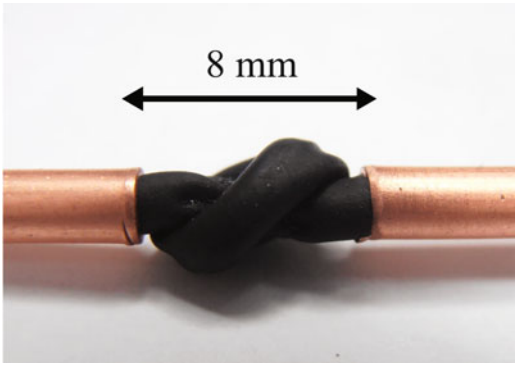

Fig. 9.1 Knot configuration—isolated knot placed between the two electrodes

9.2.2 Experimental Apparatus

The basic components of the experimental apparatus are presented in Fig. 9.2. The main system was contained in a metal frame measuring 0.8 m × 0.8 m × 2.2 m. The box was divided by a partition, such that the lower part contained the electrical system (capacitor, spark gap, and safety circuit) and the upper part housed the hydrodynamic experiment. A remotely controlled vacuum pump was used to initiate the high-current switch by pumping out the isolating gas that initially filled the box. Safety measures in the laboratory included entryway controls and interlocks.

9.2.3 Electrical Outline

The electrical system (shown in Fig. 9.2) contained three circuits, one for charging and two for discharging (one through the wire and the other through the discharge resistor). The charging circuit included a 200-μF capacitor, a charging resistor, and a 20-kV, 20-mA high-voltage power supply. The charging process was controlled remotely, and the capacitor voltage was continuously monitored. The first discharging circuit included the capacitor, the fast switch (spark gap), and the wire to be exploded. The spark gap was designed to permit high current flow in a vacuum but to be an isolator when filled with SF_6 at atmospheric pressure. By pumping the SF_6 out of the spark gap, the current stored in the capacitor could flow through the discharge circuit and explode the wire. The resistance and inductance of the discharging circuit were $R = 14$ mΩ and $L = 0.24$ μH, respectively. This created with the capacitor an under-damped RLC circuit.

To enable side and top views of the experimental apparatus, two optical high-speed flow visualization configurations were used. For the side view, two transparent PMMA windows were mounted on the experimental frame (see Fig. 9.3a). A parallel beam of light aimed through the experimental region created a shadowgraph projection of the shock fronts on a semi-transparent screen. For the top view, a beam of light entering the test chamber from the top passed through the experimental

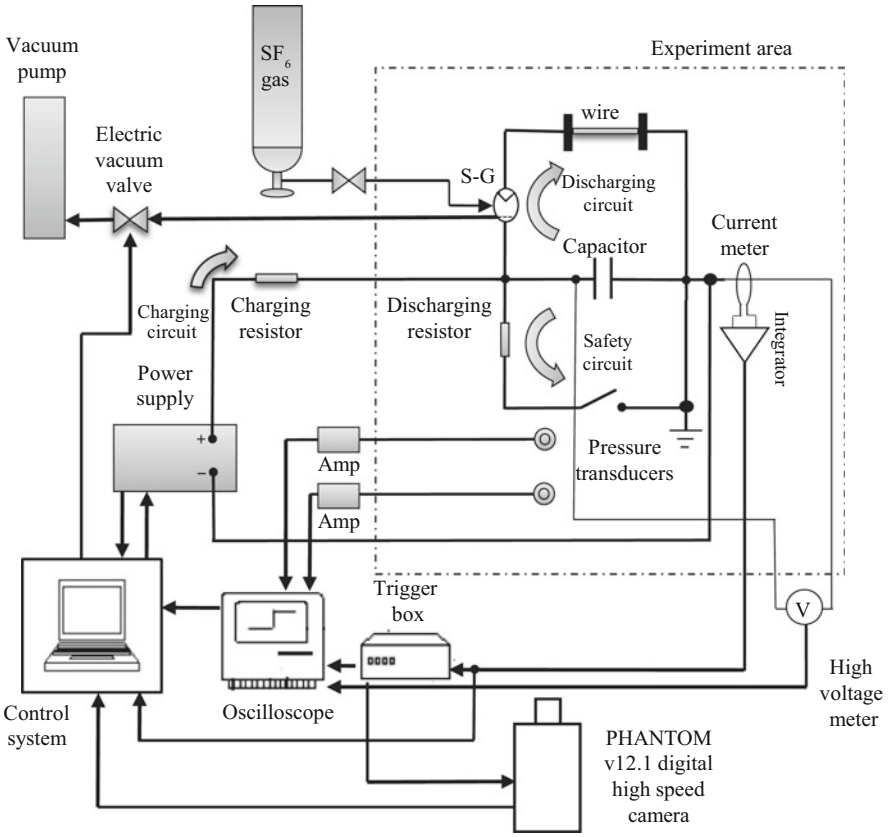

Fig. 9.2 Schematic illustration of the components of the exploding wire system in the BGU shock wave laboratory

region and created a shadowgraph projection on the floor of the test chamber (see Fig. 9.3b). The projected images were captured by the high-speed camera placed beside the test chamber via a planar mirror mounted above the explosion area. The light source for the shadowgraph setups was a double-frequency pulsed Nd^{+3}:YAG laser (532 nm) that could produce 240-ns long pulses with a repetition rate of up to 50 kHz and pulse energy of approximately 2.4 mJ. The light from the remotely situated laser entered the system room via a multimode optical fiber. The expanding light emitted from the fiber was transformed into a parallel beam with a 250-mm parabolic mirror and projected through the test area onto a screen. A high speed digital camera (Phantom v12.1) capable of capturing images at a rate of 20,000 fps with a resolution of 512 × 512 pixels was used to monitor the entire event. A 532-nm band-pass filter (10-nm wide) mounted in front of the camera was used to block the self-emission light from the wire explosion. The laser pulse rate was measured with a photodiode placed near the laser output.

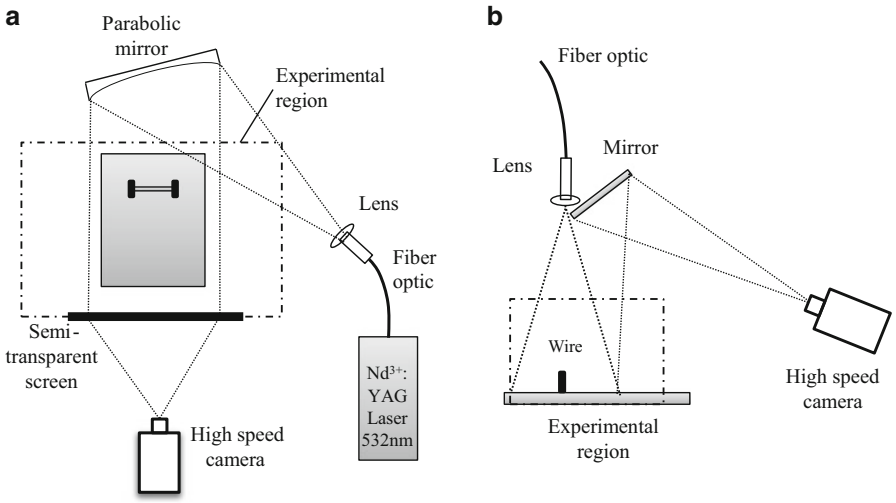

Fig. 9.3 The high-speed shadowgraph setups for (**a**) side view and (**b**) top view

The pressure history recording system was based on Kistler 211B2 and 211B3 piezoelectric transducers, which were calibrated in-house using a shock tube system. The pressure transducers mounted inside the test chamber were connected to the acquisition system, which consisted of a Kistler signal conditioner model 5118B2 and a digital oscilloscope. The current passing through the exploding wire was measured with a specially built and calibrated Rogowski coil placed around one of the conductors between the capacitor and the exploding wire. The measurement system, based on two Lecroy 314A wave-jet 100 MHz, 1 GS/s oscilloscopes, was capable of acquiring data from 8 channels simultaneously. An external trigger box was built to trigger both the high-speed camera and the acquisition system. The latter was triggered by a voltage drop in the capacitor or by the current pulse measured by the Rogowski coil.

9.2.4 Image Processing

To enhance image quality, a background image that was acquired before the shock wave was generated was subtracted from each consecutive image. This procedure enabled us to eliminate nonuniform backlight distribution and some imperfections in the windows to produce a clean image in which the wave front, flow pattern, and fragments are more pronounced. Figure 9.4, an example of the results of this procedure, shows the effect that background subtraction can have on an untreated image.

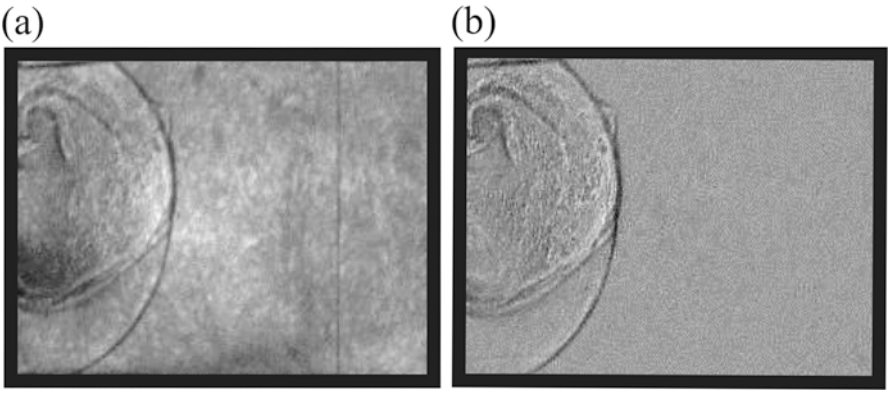

Fig. 9.4 An example of image processing results: (**a**) unprocessed image, (**b**) the same image after processing, i.e., subtracting the background image from (**a**)

9.3 Calibration

The first stage of the experiment was designed to determine the ideal operational conditions of the system. For the exploding wire configuration, two 70-mm long copper wire diameters were used, 0.9 mm and 1.1 mm. For the exploding knot configuration, a 1.25-mm wire diameter was used to ensure that a larger mass of copper was available for the explosion. The voltage and the current signals were monitored to assess the explosion process, and suitable working points, identified through trial and error, were characterized by the complete explosion of the wire with no energy left stored in the capacitor. The charging voltages for the working points were found to be 6 kV and 4.8 kV for the 1.1 mm and 0.9 mm wires, respectively, and for the exploding knot the used voltage was 4.5 kV. To measure the strength of the explosion, a pressure transducer was mounted on a movable stand placed in front of the explosion at distances ranging from 40 to 150 mm. For the experiments with exploding knots, the measurements were compared to CONWEP generated results (CONWEP 1992). In an iterative process it was found that the equivalent amount of TNT that gave similar results was 60 mg (in spherical charge geometry). A numerical simulation had to be used in order to find the energy embedded in the blast wave in the exploding wire experiments. An axis-symmetric numerical simulation was solved using the MSC/Dytran solver (2008r1). To simulate a cylindrical explosion, a high density cylindrical bubble with high internal energy was placed in the explosion position under ambient conditions. We used an iterative process to determine the conditions that promoted generation of the blast wave by the exploded wires. The results obtained from the wire experiments were fitted to the theoretical cylindrical model of Lin (1954) given by Eq. (9.1),

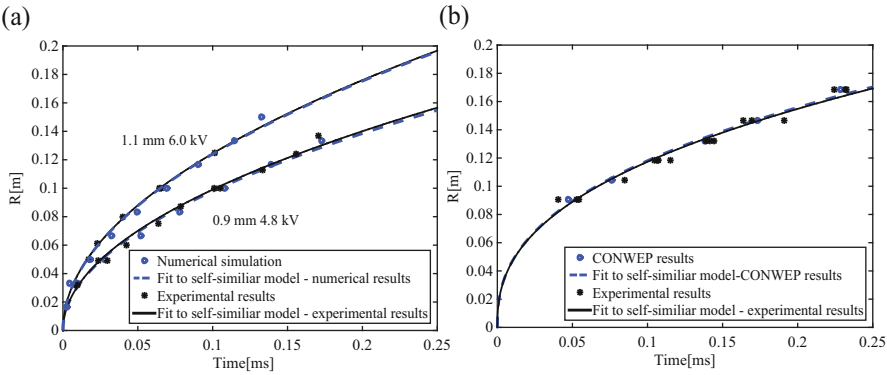

Fig. 9.5 Comparison between the numerical and the experimental results that were used in the calibration procedure

Table 9.1 The charge energies and the energies embedded in the blast waves that were found using the calibration procedure for the three working points

Experimental configuration	Charging voltage (kV)	Capacitor charged energy (kJ)	Calculated embedded energy
1.25-mm knot	4.5	2.25	0.3 kJ
1.1-mm wire	6.0	3.6	1.14 kJ/m
0.9-mm wire	4.8	2.3	0.33 kJ/m

while those obtained from the knot experiments were fitted to the theoretical model of Taylor (1950) given in Eq. (9.2):

$$R(t) = A\,(E, \rho, \gamma) \cdot t^{\frac{1}{2}} \tag{9.1}$$

$$R(t) = B\,(E, \rho, \gamma) \cdot t^{\frac{2}{5}} \tag{9.2}$$

where $R(t)$ is the radial position of the incident blast wave, t is the time, and $A(E, \rho, \gamma)$ and $B(E, \rho, \gamma)$ are constants that depend on the energy of the explosion ambient density and the heat capacities ratios. The energies found to fit the wire experiments best were 0.33 and 1.14 kJ for the lower and higher working points, respectively. Comparisons between the experimental and numerical results of the exploding wire and knot experiments are presented in Fig. 9.5a, b. Table 9.1 summarizes the charge energies and the energies embedded in the blast waves that were found using the calibration procedure for the three working points.

Once the energies embedded in the explosions have been found, the symmetry of the spherical blast created by the knot was examined. The blast wave fronts images taken from side and top views were fitted to a circle. The fitting showed that the exploding knot produced a perfectly spherical explosion (see Fig. 9.6).

The head-on pressure history was measured by a pressure transducer flush mounted on a perpendicular stand at a height of 70 mm above the floor, which was the height of the explosion. The distance between the pressure transducer and the explosion was 118.5 mm. The setup configuration is shown in the inset in Fig. 9.7. The measured reflected pressure history from a pressure transducer was compared to

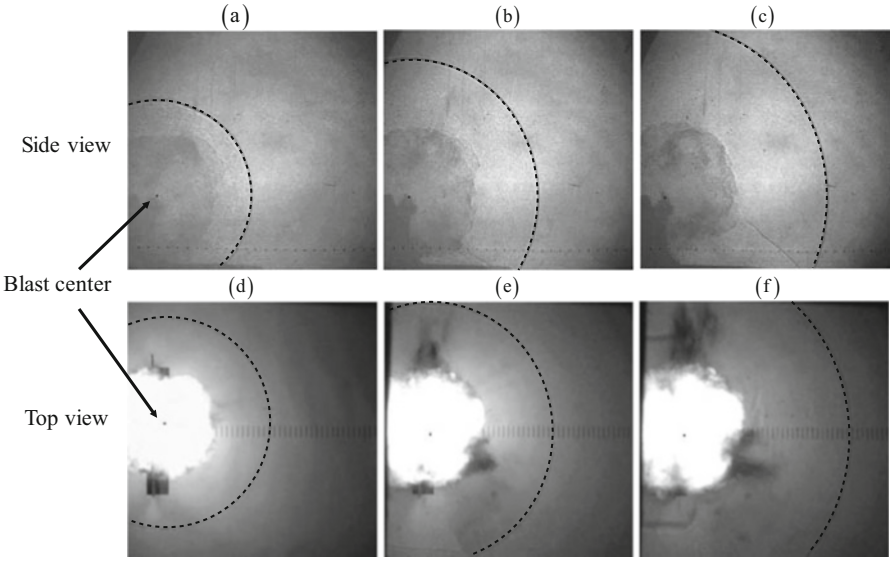

Fig. 9.6 Results of the exploding knot experiment: (**a–c**) side view; (**d–f**) top view. The fitted circles are superimposed on the images and are plotted as dashed lines. The dots shown in each of the figures (**a–f**) represent the blast center as found by the fitted circle

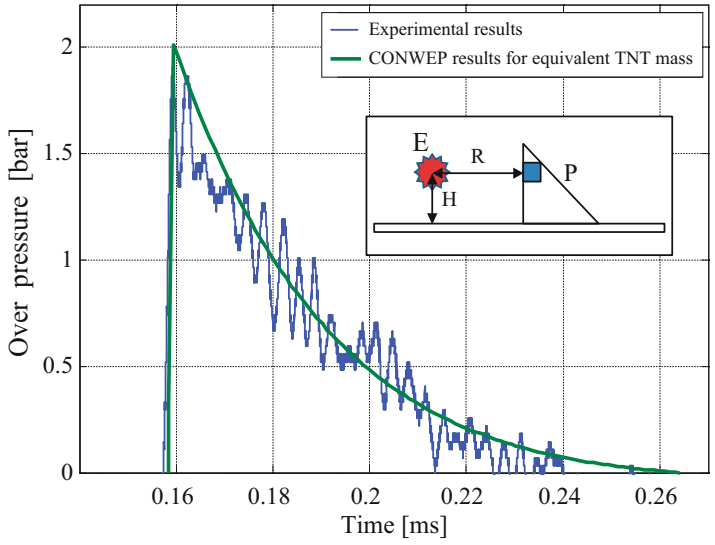

Fig. 9.7 A comparison of pressure histories between the CONWEP and the experimental results. Inset: measurement configuration: P-pressure transducer, E-explosion, $R = 118.5$ mm, $H = 70$ mm

a CONWEP generated pressure profiles. As can be seen in Fig. 9.7 good agreement was found between the pressure histories generated by the exploding knot and the CONWEP results.

9.4 Results

In the following, two experimental studies demonstrating the capabilities of the exploding wire facility to investigate the interaction of small-scale cylindrical and spherical blast waves with complex structures are presented.

9.4.1 Case A: The Interaction of a Cylindrical Blast Wave with a Two-Story Building

To demonstrate the suggested methodology to predict blast loads and to validate the numerical simulation, a simple but nontrivial experiment was designed. It was shown that the experimental apparatus is capable of producing 2D and 3D blast waves. To demonstrate the effectiveness of the experimental system a simple 2D case was tested. The experimental results were compared to the numerical results of a simple 2D numerical solver in which a simple Euler scheme was used to help explain the discrepancies observed between the experimental and numerical results. A comparison of the experimental results to the numerical model solved under the same conditions could enable one to deduct the strengths and the weaknesses of the numerical code.

The following sections present the test model, experiments, and numerical model, and the comparison between the results reveals the effectiveness of using such a system.

9.4.1.1 Numerical Approach

As mentioned, this study aimed at demonstrating the effectiveness of using an exploding-wire-based experimental system to predict blast loads and to validate numerical simulations. To that end, we chose, as a test case, to solve a numerical model using the MSC/Dytran commercial solver (2008r1), which is capable of solving fully coupled fluid and solid conservation laws in both Eulerian and Lagrangian mesh grids. For the purposes of this study, a second order solver was chosen that solved the Euler equations for the fluid phase, and the solid structures were assumed to be infinitely rigid. Furthermore, in the numerical model the exploding wire was replaced by a high density, high energy cylindrical gas bubble situated in the blast location. The method of using a compressed hot gas bubble to generate the exploding wire conditions in simulations was examined by Higashino et al. (1991), who found that it provided very good results. The hot gas bubble and the surrounding atmosphere were modeled as an ideal gas, and a simple γ-law was used for the equation of state of the gas. Special considerations about the numerical grid element size were made to ensure that the blast waves generated in the simulation were correctly modeled. The mesh was refined to the point at

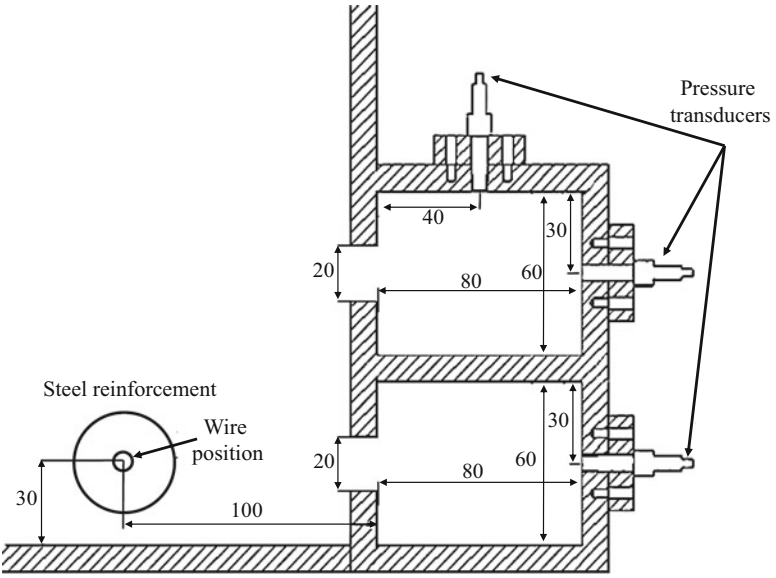

Fig. 9.8 Schematic illustration of the small model (dimensions are in mm)

which further refinement had no influence on the solution. To simplify the numerical solution and maintain the accuracy that is required to ensure good comparisons with the experimental results, the dimensionality of this test case was chosen as two.

9.4.1.2 The Test Model

The exploding wire produced a cylindrical blast wave. Its confinement between two parallel planar walls preserved the two-dimensional nature of the blast wave until later times. The small-scale model presented in Fig. 9.8 was designed as a generic two room structure, in which the rooms are placed in a two-story configuration. The room dimensions in the model were 80-mm long by 60-mm high. Since the blast waves generated using exploding wires were cylindrical, the experiment was designed to be two dimensional. The entire model was confined between two parallel walls and the wire was placed horizontally outside the structure, 100 mm in front of the lower room entrance. The entrances to the two rooms spanned the whole width of the model in order to ensure that the two-dimensional nature of the event was preserved. Three Kistler 211B2 pressure transducers were flush mounted on the first floor wall, the second floor wall, and the second floor ceiling. The model was built from nonconductive plastic to prevent circuit short. The walls proximate to the wire were opaque to block the light emitted by the explosion while those inside the rooms were transparent to enable photography. The wire entrance holes were reinforced with steel to prevent damaging the plastic walls by the experiment.

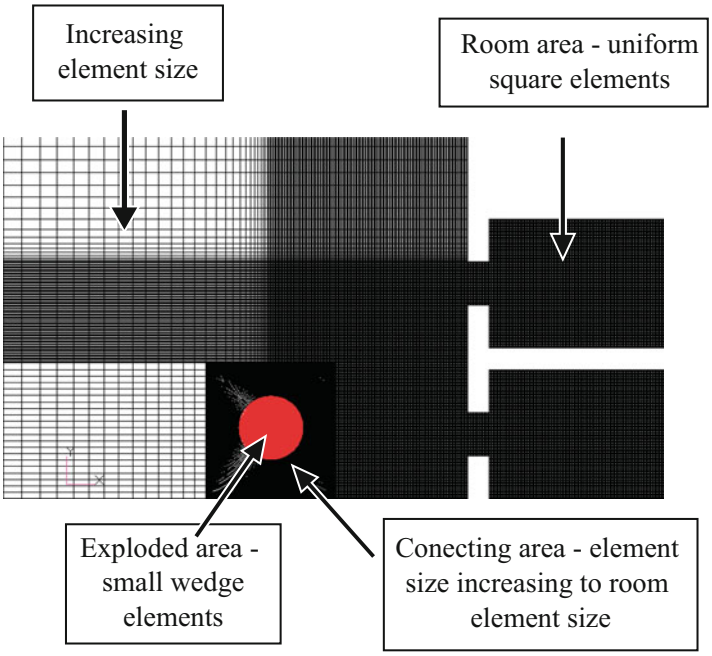

Fig. 9.9 Grid description of the solved numerical model

The grid of the numerical model shows that in the vicinity of the exploding region, the mesh in and between the rooms is gradually refined to permit high accuracy (see Fig. 9.9). The mesh inside the rooms was a 0.5-mm × 0.5-mm Cartesian grid while that outside the rooms was biased to allow element sizes to grow with the distance from the explosion area. Here also the explosion area was mimicked by placing a hot, dense cylindrical bubble in the exploded wire location.

9.4.1.3 Comparison of Experimental and Numerical Results

The experimental data acquired for the tested scenario enabled the examination and validation of a numerical model.

In contrast to full-scale experiments, in this laboratory scale test the implementation of a variety of accurate diagnostics yielded an amount of data that permitted performing a detailed comparison. The resulting visual images enabled a very good qualitative comparison to the numerical simulations, and the direct pressure measurements enabled a quantitative comparison. A series of experiments was performed using a 1.1-mm wire at 6 kV (the higher working point). Shadowgraph images taken in the experiment and shadowgraph representations obtained from the numerical solution are presented in the left and right panels of Fig. 9.10, respectively.

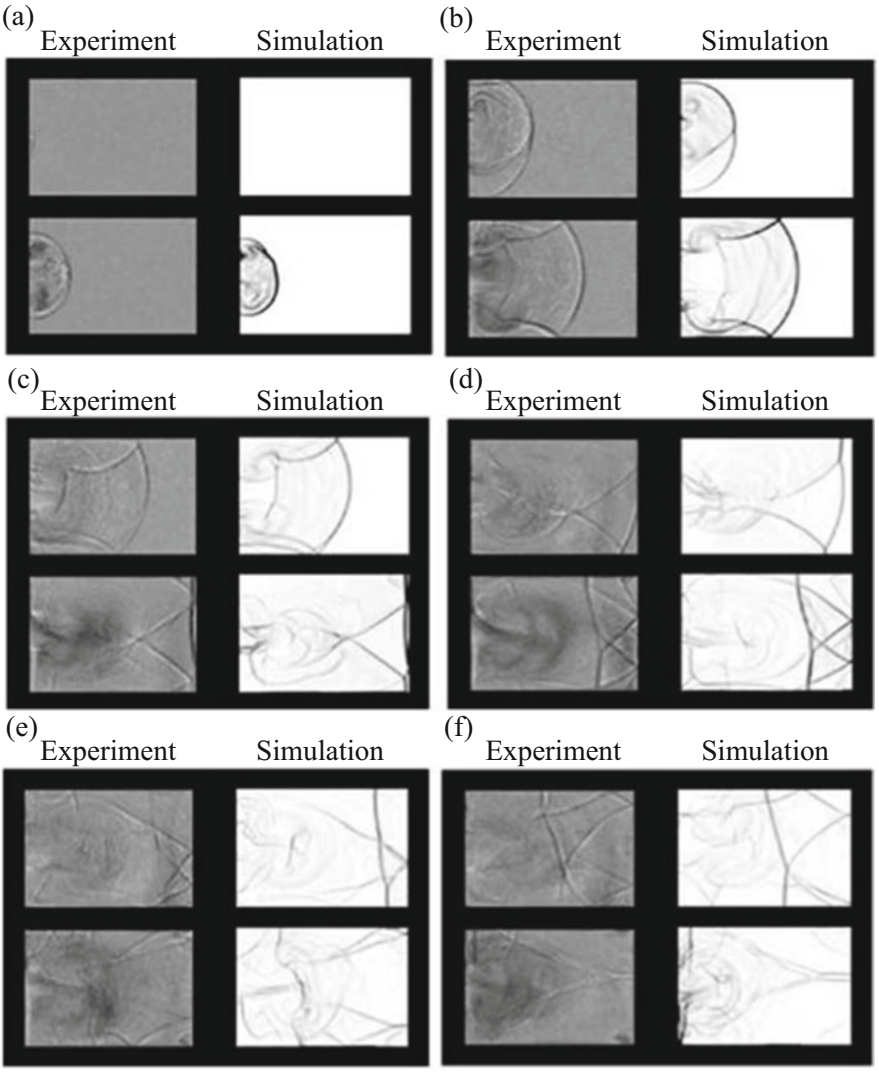

Fig. 9.10 Qualitative comparison between numerical (**a–f**, right panels) and experimental (**a–f**, left panels) results

The qualitative comparison shows that the results obtained from the numerical simulation were in good agreement with the experimental results. The incident blast waves that entered the rooms had similar characteristics in terms of, for example, their interaction with the structure and the intricate features of the different reflection phenomena. After a certain time, however, slight discrepancies emerged between the numerical and experimental results. Also, although the features of the reflections behind the incident blast wave were identical to those in front, their

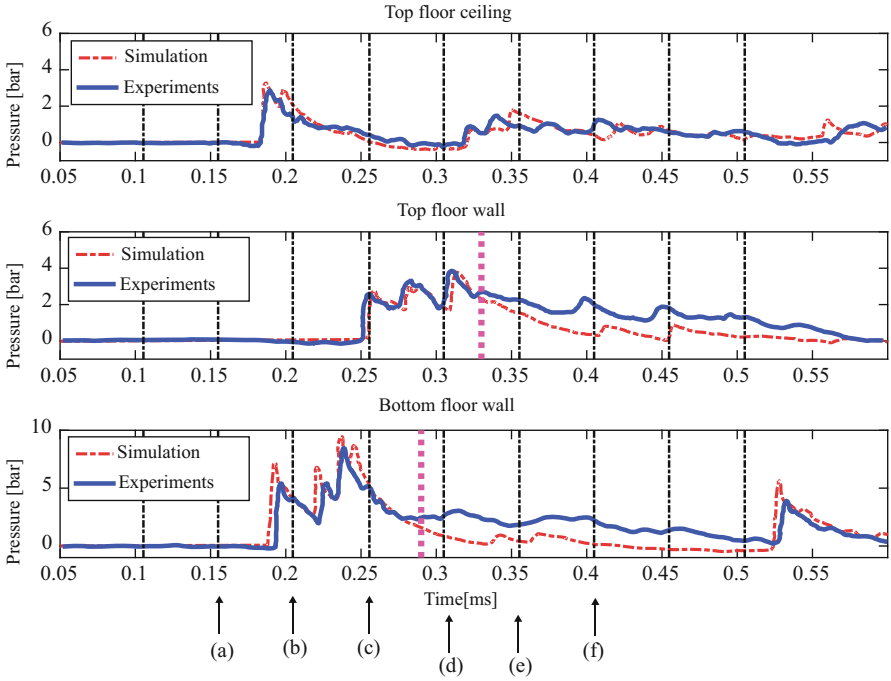

Fig. 9.11 Pressure comparisons between numerical and experimental results

locations were slightly different. A quantitative comparison of pressure history measurements to the corresponding results from the numerical simulation shows a discrepancy between the numerical and experimental results (Fig. 9.11). As the experiment progressed, the experimental pressure diverged from the calculated pressure at different times for the second floor wall and first floor wall measuring points (marked on the graphs with heavy dashed lines), but no such deviation was observed for the second floor ceiling.

9.4.1.4 Discussion and Conclusions

The foregoing described research demonstrated the use of an exploding wire technique to study blast wave–structure interaction. The experimental setup facilitated the implementation of sophisticated and sensitive diagnostics that permitted quantitative and qualitative comparisons with numerical tools. For the test case presented, it was shown that some discrepancies existed between the experimental and numerical results. A close examination of the results elicited a possible explanation for these discrepancies. An analysis of the captured images and the pressure history showed that the deviations between the two sets of results began after the interaction of the blast wave with the vortex created by the incoming flow.

It is clear that in its late stages, the interaction was not simulated correctly due to numerical limitations such as limited resolution, viscosity, and turbulence that were not accounted for, and three-dimensional effects. Furthermore, examining the pressure histories with the added information obtained from the images revealed that the waves traveling alongside the ceilings of both rooms were affected less by the incoming flow from the entrances. The pressure history on the second floor wall is in better agreement with the simulation due to this weaker interaction.

To apply this small-scale experimental system to full size structures, Kleine et al. (2005), Neuberger et al. (2007), Smith et al. (1992), and others have previously stated and demonstrated the ability to predict blast loads on full-scale structures based on the results of small-scale experiments. The common method of scaling a spherical explosion is the well-known Cranz-Hopkinson's "cube root" scaling law, which states that two similar geometries and charges that have different charge weights can be scaled using the cubic root of the charge energy. As shown in Baker (1973), the scaling parameters are:

$$\begin{aligned} Z &= \frac{R}{E^{1/3}}, \\ \tau^* &= \frac{\tau}{E^{1/3}}, \\ \zeta &= \frac{I}{E^{1/3}}, \end{aligned} \tag{9.3}$$

where Z is the scaled distance, τ^* is the scaled time, ζ is the scaled impulse, R is the radius from the explosion source, and E is the charge energy that can be replaced by the charge weight. Using these scaling parameters and a spherical rather than a cylindrical blast profile in the experiment, this scaling law can be used to scale up experimental results. Furthermore, using this scaling law, blast velocity, the pressure jump, and medium density are the same for the small- and full-scale setups, which leads to identical Mach and Euler numbers in both setups. These nondimensional numbers are highly relevant to this problem, where viscosity effects are negligible. In this case the two setups are similar and similitude is achieved.

9.4.2 Case B: The Dependency of the Load Penetrating into a Structure on the Initial Conditions and the Internal Geometry

Studies regarding shock and blast wave interaction with structures from a protective standpoint can be divided into two main groups. The first group includes studies that are more fundamental, where the impingement of a shock or blast is studied with regards to a specific element for purposes of either studying its response or to study the attenuation or enhancement properties of the element. The second group focuses on the load developing and the response of a structure subjected to an explosive event. While the first group usually deals with the physical mechanisms of shock structure interaction, developing flow fields and material response, the second group

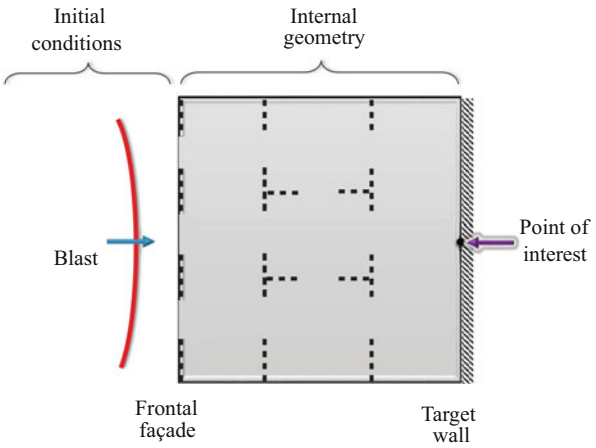

Fig. 9.12 The investigated problem. A blast wave impinging the frontal façade of a one-story building generates the pressure and impulse initial conditions. The blast propagating inside the structure is affected by the inner geometry. The point of interest is located at the center of the back wall

includes studies that are more typically focused on the application to structural design, load assessment, and survivability following an explosion event.

9.4.2.1 The Investigated Problem

This study aims to improve the understanding of the physical mechanisms determining the pressure buildup inside a structure following the impingement of an explosion-originated blast wave. Figure 9.12 broadly renders the important aspects of the studied problem. The study focuses on a single-story building exposed to a blast wave impinging on its frontal façade. The blast wave generates initial conditions on the frontal façade of the structure, namely pressure and impulse. Typically, following the initial impingement, a weaker blast wave enters the structure through the openings in the frontal façade, propagates through the structure, and reaches the back wall. Throughout its propagation, the initial wave diffracts and reflects off the internal walls. The diffracted waves reverberate throughout the structure, with some pressure exiting from the building façade openings, until eventually the reflections subside and the pressure returns to the atmospheric level. The main point of interest in this study was located along the structure's symmetry line, as shown in Fig. 9.12.

Resolving the three-dimensional diffraction pattern inside the complex structure is difficult and resource consuming. Furthermore, the wave propagation inside the structure and the resulting flow field highly depend on the internal geometry. Accurately resolving the internal flow field numerically for every change in the initial conditions or internal geometry would require a new simulation.

Rather than studying the detailed flow features and reflections, this study adopted a different approach to studying the pressure buildup dependency on the important parameters. We examined the scenario presented in Fig. 9.12 in terms of initial conditions, internal geometry, and target wall pressure. This approach considered the internal geometry (boundary conditions) as an element that modifies the initial pressure and impulse inflicted on the frontal façade and compares it to the load inflicted on the target wall.

9.4.2.2 Initial Conditions

Maintaining a constant explosion yield by using identical wires enables two possible ways to set the initial conditions imposed on the frontal façade of the structure (see Fig. 9.13). The first is by changing the frontal façade distance from the free air explosion. As the distance increases, the blast decays along with the imposed pressure and impulse. This method is effective but each distance generates a change in both the pressure profile and the impulse. A second method employs a stiff reflector placed around the explosion, which channels more energy towards the target. This method yields a different pressure—impulse combination than in the free air case.

The reflector permitted finding "semi-equivalent" initial conditions where the peak impulse generated at a specific distance from the free air explosion was the same as that generated with the reflector but at a different distance. For

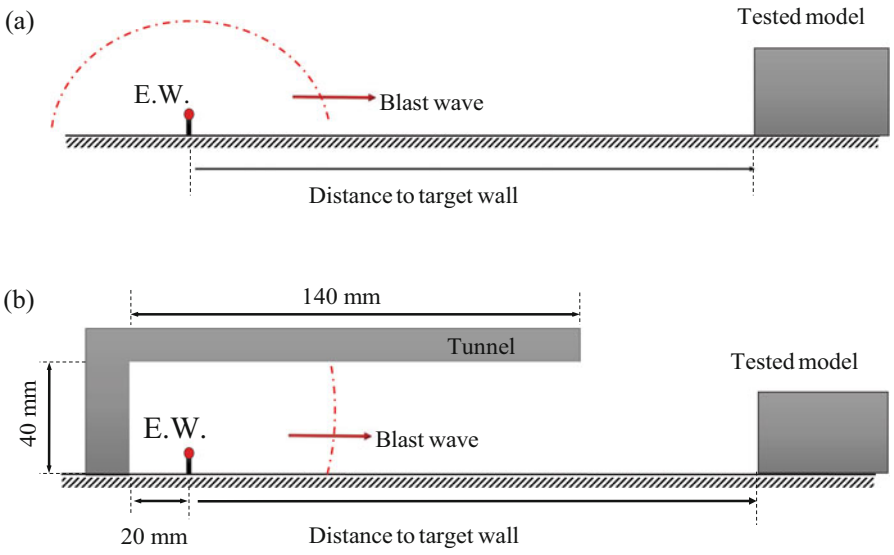

Fig. 9.13 The two methods chosen to generate the initial conditions: (**a**) Open-air ground-burst; (**b**) A reflector around the explosion area that channels more energy towards the structure

example, one combination used in this study was free air at 100 mm from the explosion and 300 mm from the explosion with the reflector. In these locations, the peak impulses were very similar though the peak overpressures were different. Though nonintuitive, this comparative method enabled the separation of one initial parameter: impulse or pressure.

The reflector was 40-mm high and 140-mm long. The gap between the inside back wall of the reflector and the exploding wire was 20 mm. All the experiments that were performed in this study were done using copper wires that were 70-mm long and 1.1 mm in diameter. The charged capacitor voltage was 6 kV for all of the experiments.

9.4.2.3 Repeatability

Explosions generated by the exploding wire technique are highly repeatable. The main parameters affecting the explosion strength are the wire material, wire dimensions, and the energy stored in the capacitor. To check the system repeatability, three experiments were conducted under the same conditions. The reflected pressure and impulse from these experiments measured at 150 mm from the explosion are presented in Fig. 9.14a, b, respectively. These results demonstrate the very good repeatability of the system and hence in the subsequent analysis each experiment appears only once.

9.4.2.4 Internal Geometry

Figure 9.15 depicts four different structure models used in this study. Each model had the same frontal façade spanning 92 mm by 25 mm (including external walls) with three 12 mm by 10 mm equally spaced windows. The models differed as follows:

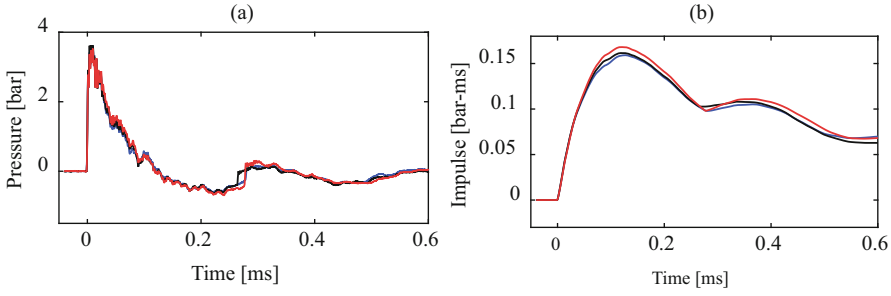

Fig. 9.14 Reflected pressure and impulse measured 150 mm from the explosion in three different experiments

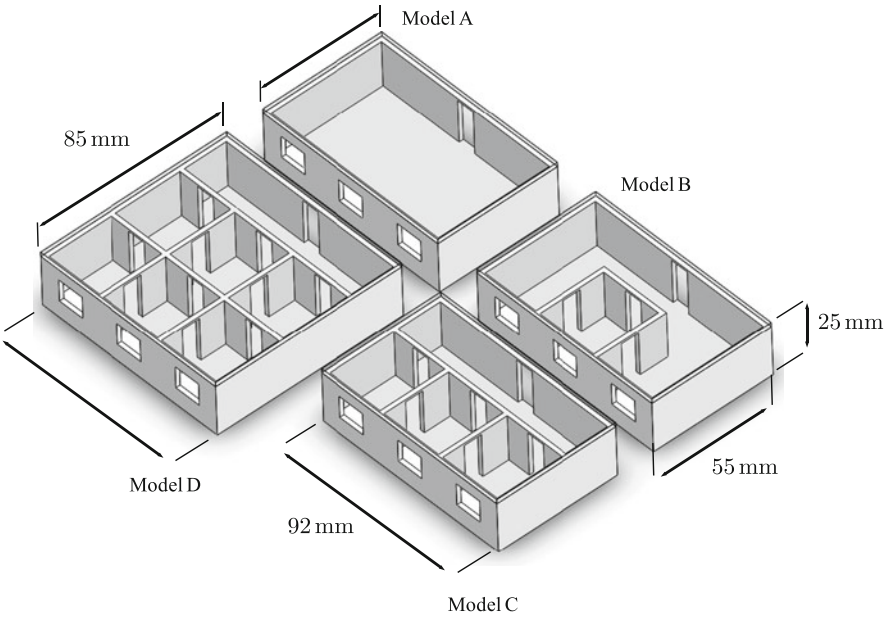

Fig. 9.15 Four one-story structure models ranging in size and in internal geometry

- Model A had no internal divisions.
- Model B had a 28 mm × 28 mm centered room partially obstructing the flow immediately behind the center window, in addition, an 8 mm × 20 mm doorway was located in the center of each internal wall.
- Model C had three internal rooms each 28 mm × 28 mm placed immediately behind the frontal façade wall. A doorway connected each pair of adjoining rooms and three more doorways were placed facing the façade and in symmetry with the three windows. All doors were 8 mm wide and 20 mm high.
- Model D was 85 mm long and had an additional row of internal rooms identical to the row of rooms in model C.

All the model parts were machined out of 2-mm thick polycarbonate sheets. The parts were then glued together assuring a tight seal. The models were positioned with the frontal façade directly facing the exploding wire at various distances. A pressure transducer (Kistler 211B3) was mounted on a wall adjacent to the target wall at the door opening (see schematic illustration in Fig. 9.16). The height and width of the mounting wall matched the structure so as not to influence the flow with the formation of external reflections.

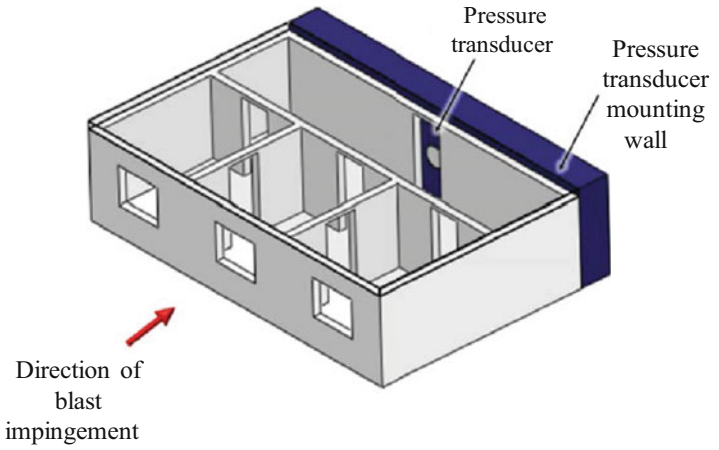

Fig. 9.16 Schematic description showing the pressure transducer mounted at the center of the opening in the target wall

9.4.2.5 Results

Two sets of experiments were performed in order to study the individual influence of the initial conditions and the internal geometry. In the first set, the internal geometry was varied while maintaining the initial conditions constant. In the second set, each model was subjected to varying initial conditions; a model was placed at a certain location, exposed to an open air explosion and then moved to a farther location with the reflector so that the imposed peak impulse was similar to the one measured in the closer open air experiments. The following sections aim to highlight the effects of each parameter.

Effects of the Internal Geometry

Figure 9.17 depicts the results obtained by exposing models A, B, and C to an open-air explosion with the model frontal façade placed at 150 mm from the explosion. Figure 9.17a, b contains the initial conditions; the measured pressure profile and impulse measured on the frontal façade before the effect of the internal geometry. These measurements were performed by mounting the pressure transducer at a distance of 150 mm from the explosion without the present of a model. Figure 9.17c, d presents the measured pressure and impulse profiles at the point of interest, i.e., the opening in the center of the target wall. To enable direct comparison between the results, all the presented recordings are shifted in time so that time $t = 0$ is when the incident wave reaches the transducer.

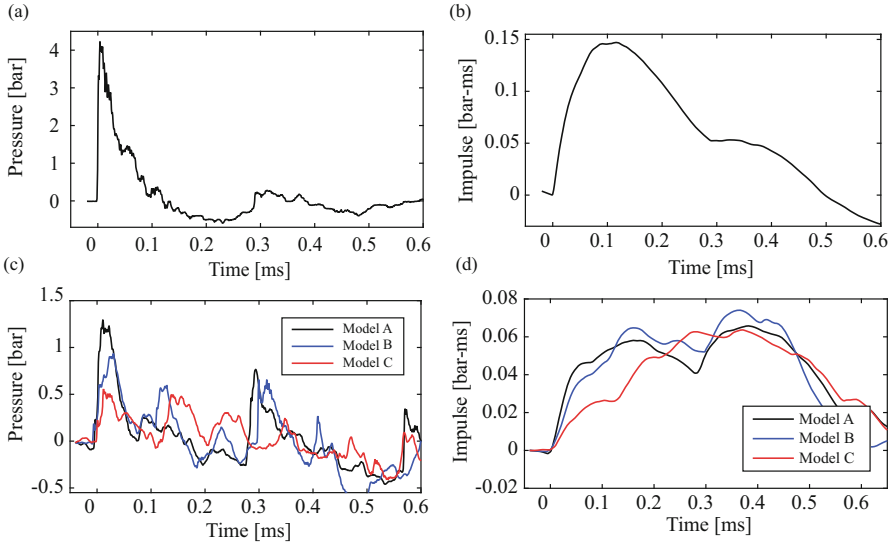

Fig. 9.17 Results from experiments performed with various internal geometries. (**a**, **b**) depict the reflected pressure and impulse developing at the frontal façade of the structures measured at 150 mm from the explosion without a model; (**c**, **d**) depict the pressure and impulse measured at the center of the target wall in each of the models A, B, and C

The results in Fig. 9.17 show that the overall measured impulse behavior at the target wall is similar in all of the experiments. As the models become more complex such as with model C we notice some changes in the impulse buildup, but still the overall behavior and peak impulses remain almost the same. Since each structure had the same windows at the frontal façade and the same initial conditions, the mass flux into the room and the incoming blast wave were also the same. The pressure profile, on the other hand, was highly influenced by the internal geometry. For example, Fig. 9.17c shows the reflection pattern through model A, a structure without internal divisions. The initial shock is measured arriving at the target wall and then reverberates between the frontal façade and the back wall. The arrival of this trapped shock produces definitive pressure jumps where there are only weak secondary reflections from the walls reaching the measurement point in between. In the experiments with model C, a significantly more complex structure, a pressure history featuring many shock reflections is visible. These weaker pressure jumps are accompanied by many minor reflections, which are probably transverse waves emanating from the interaction with internal walls.

A second effect revealed in Fig. 9.17c is that the initial pressure jump caused by the initial shock propagation strongly depends on the complexity of the inner geometry. The peak over pressure diminishes with exceedingly complex geometries. Subsequent reflections seem to be more similar in strength between the models.

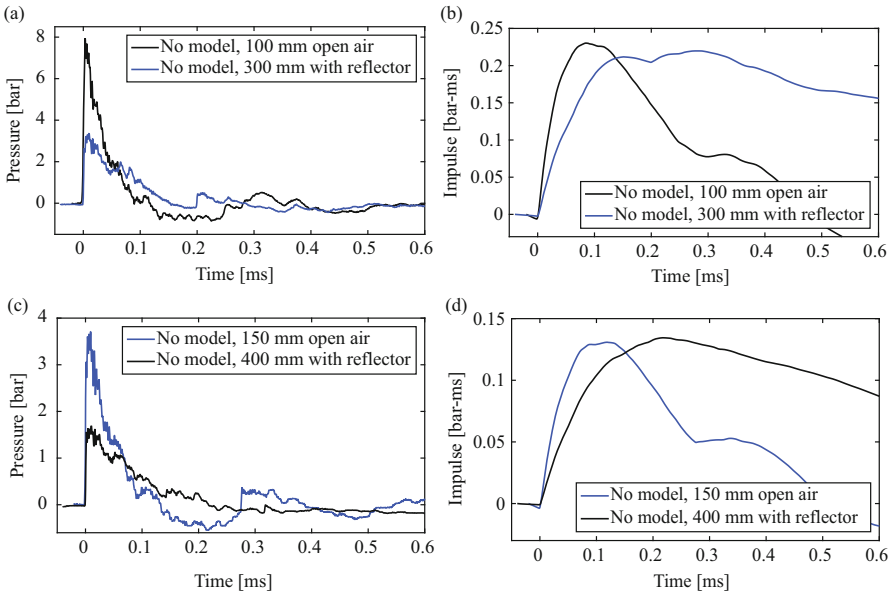

Fig. 9.18 Comparison of the pressure-impulse combinations that were obtained in open air and with reflector explosions. The explosion with reflector provides a peak impulse at a certain location that matches that of an open-air explosion at a closer location

Effects of the Initial Conditions

A second set of experiments was performed to study the effects of the initial conditions on the pressure buildup at the target wall. As stated previously, changing the distance between the exploding wire and the model frontal façade alters the initial conditions. The impulse and pressure change in different manners, and hence this method offers no comparable data. An alternative method overcomes this limitation. A reflector, shown in Fig. 9.13b, focuses the blast energy thereby providing at a certain location a peak impulse that matches that of an open-air explosion at a closer range. Figure 9.18 presents two combinations of open-air and reflector explosions. It is impossible to generate the same impulse history at the frontal façade, but Fig. 9.18 depicts two combinations that generate impulses sufficiently similar for our purposes, especially when the peak impulse is concerned.

The two combinations shown in Fig. 9.18 generate similar *peak impulses* on the structure while imposing very different pressure loads both in peak over pressure and in the duration. It is important to note that the peak impulse is reached when the positive pressure duration ends, i.e., the pressure returns to atmospheric conditions. Since the open-air explosion generates an additional negative pressure phase, the impulse declines much faster. This effect, however, has little influence on the conditions inside the structure since low pressure propagates inwards at a slower speed. The mass flow into the structure effectively stops when the impulse begins to decline.

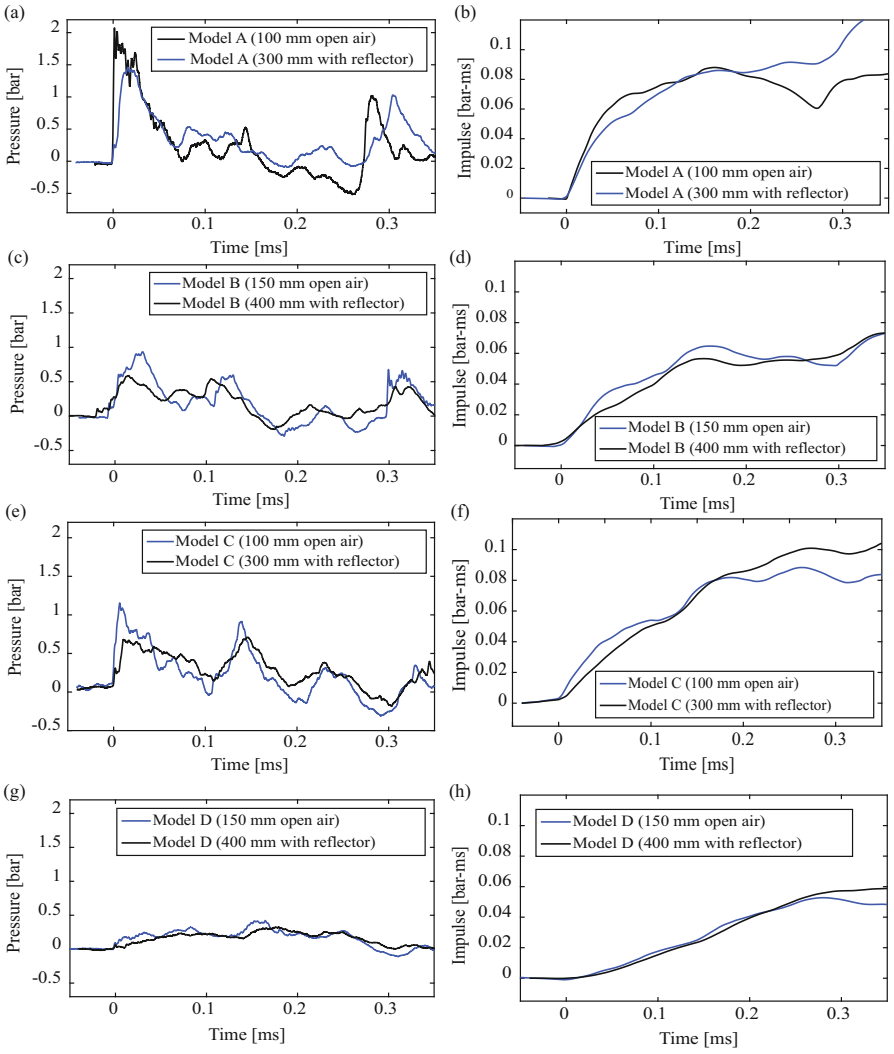

Fig. 9.19 Experimental results depicting the target wall pressure and impulse profiles in the various models. The experiments were performed with different initial conditions in which the inflicted peak impulses were kept similar

The initial conditions shown in Fig. 9.18 were inflicted on the models shown in Fig. 9.15 by placing the façade at the same location where they were measured (the pressure transducer mounting wall was placed at different locations accordingly). Figure 9.19 depicts the over pressures and impulses measured at the end wall of models A, B, C, and D. A single set of initial conditions is presented for each model.

As expected, since the two impulse initial conditions were similar up to the peak, the impulses on the target wall are also in a reasonable agreement. In the open-air

experiments, the low pressure propagates into the structure and lowers the impulse after the peak as seen in the initial conditions (Fig. 9.18).

The pressure measurements recorded at the target walls, on the other hand, are not so intuitive. Despite very different initial pressures inflicted on the façade for the open air and reflector explosions (up to twice the peak over pressure), the pressure profiles inside the structure were remarkably similar. In fact, the pressure profiles display similar over pressure as well as similar reflection patterns. To explain this, we refer to the results shown in Fig. 9.17. We saw that imposing the same initial conditions in terms of both pressure and impulse caused the impulses at the target wall to match but with very different reflection patterns. In this case, the dominance of the internal geometry is even more pronounced since the reflection patterns are not only highly affected by the internal geometry but also impede the propagation of stronger shocks inside the structure. To support this notion, a comparison between two different internal geometries shows that as the complexity increases the pressure profiles become even more similar.

9.4.2.6 Application to Large Explosion Modeling

The above findings have valuable implications for simulating large explosion in laboratory settings. Though very repeatable and easy to employ, the exploding wire method generates weak explosions. A previous study showed that at the system used here, i.e., exploding a 70-mm long, 1.1-mm diameter copper wire with 6 kV in the capacitor generates an energy equivalent to the explosion of 0.1 g of TNT (Ram and Sadot 2012). Consequently, simulating large explosions in urban scenarios, such as one ton of TNT, would necessitate scaling down to miniscule proportions. The results here provide a tool to address this problem.

To demonstrate the implications of the results shown above, a full-scale simulation of an explosion event at which an 800 kg TNT charge explodes 15 m from the frontal façade of a structure is evaluated. Figure 9.20 depicts the overall dimensions of the full-scale scenario. The structure has three equally spaced 1 m × 1 m windows at its frontal façade, and two 1 m × 2 m windows at its sides. Inside, a 3 m × 3 m room was located adjacent to the frontal façade, behind the center window, partially obstructing the path to an opening at the target wall.

Fully scaling down the model, by means of the Cranz-Hopkinson law, to meet the exploding wire system capabilities requires an impracticably small model (in the order of 1:1000). The model would be so small that the pressure transducer could not fit the opening at the target wall.

In light of this restriction, we chose a more feasible small-scale ratio of 1:100 to simulate the explosion by means of the exploding wire system. Properly simulating the explosion would further require creating a scaled down 0.8 g hemispherical explosion at a distance of 150 mm from the frontal façade of a scaled down model. Since we could not satisfy these conditions under the exploding wire system limitations, we used the reflector and found the location where the produced impulse matched a 0.8 g TNT explosion at a 150 mm range. The desired pressures and

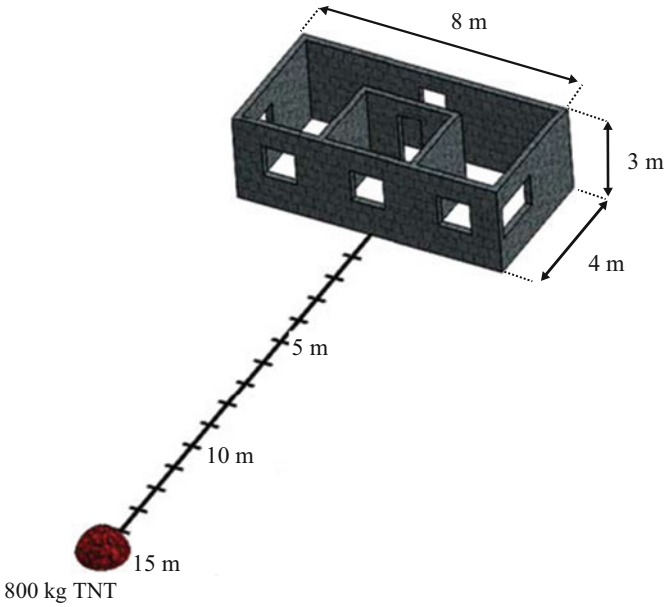

Fig. 9.20 The full-scale scenario in which an 800 kg hemispherical TNT charge explodes 15 m from a one-story structure façade. (The roof is transparent)

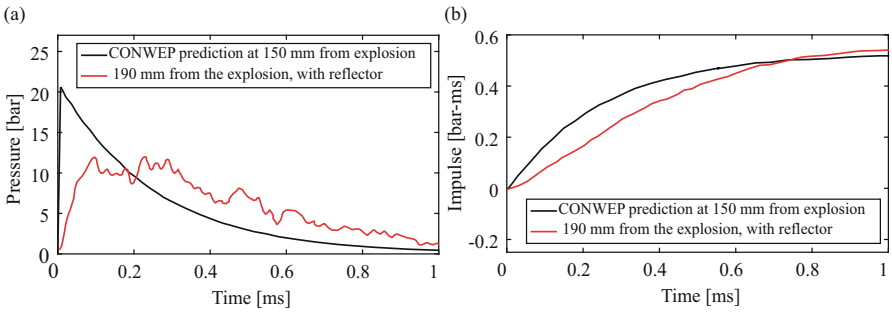

Fig. 9.21 Pressure and impulse profiles required to simulate an 800 kg explosion in a 1:100 scale. The desired conditions are that of a 0.8 g TNT charge detonated 150 mm from the model. The closest conditions were found using the reflector at 190 mm from the exploding wire

impulses were obtained by means of the CONWEP software (1992). Figure 9.21 depicts the closest match that was found, at a distance of 190 mm from the exploding wire. As concluded in Sect. 9.4.2.5 we selected the distance that provided the most similar impulse.

Numerical simulations of the full-scale model were performed using MSC/Dytran commercial software. The numerical model was validated with full scale experiments and was found to be in good agreement (Ostraich et al. 2009)

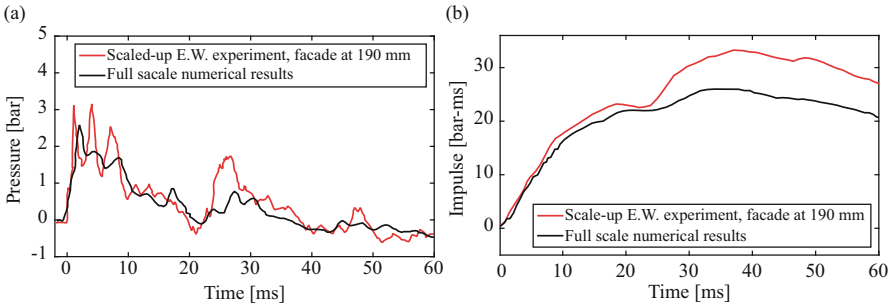

Fig. 9.22 A comparison between a numerical simulation and an exploding wire experiment at the target wall. While the initial imposed conditions on the frontal façade only matched in terms of impulse. A very good resemblance was found in both the impulse and the pressure at the target wall

with them. In order to simplify the numerical model it was assumed that during the initial wave propagation inside the structure the walls were non-deformable. A symmetry assumption was also used and only half of the structure was simulated. The explosion was modeled as a hot air bubble burst calibrated to yield the appropriate TNT equivalent (Ram and Sadot 2012). The blast loading on the building frontal façade was validated by CONWEP predictions, which also yielded satisfactory agreement.

The small-scale model was built from polycarbonate sheets in the same manner as the previous models were made and placed in the exploding wire system. Figure 9.22 shows a comparison between the experimental results and numerical simulation of the full-scale experiments. To display the comparison, the pressure and the impulse histories from the small-scale experiments were scaled up according to the Cranz-Hopkinson law to the full-scale simulation.

The small-scale experiment and the numerical solution agree in both impulse and pressure. It could be expected that by tailoring the impulse imposed on the façade we should get the proper impulse at the target wall. However, an agreement between the pressure profiles was not initially expected but could be explained based on the results presented in the previous section. The impulse transfer through the structure along with the internal geometry assured that the pressure profile was very similar to the one recorded in the simulation regardless of the incorrect pressure imposed on the frontal façade.

9.4.3 Conclusions

The current study empirically explored the effects of initial conditions and internal geometry on the pressure developing inside a single-story building. It was found that when inflicting similar impulses at the frontal façade of the structure, the internal

geometry determines the pressure profile that develops at the target wall regardless of the initial pressure profile.

These inferences were applied to the experimental study of a blast event in a small-scale setup. The presented findings imply that in the case where the load developed in an interior of a complex structure by exterior blast event is of interest, it is satisfactory to impose the correct impulse at the façade to acquire adequate results in terms of both impulse and pressure inside the structure.

Furthermore, as the complexity of the structure increases, the larger number of reflections facilitated by the internal divisions contribute to the independency of the target wall loading in the imposed pressure profile. The results show the consistency of this phenomenon and will in the future enable faster examination of protective structures in laboratory settings.

9.5 Final Remarks

The experimental system presented in this chapter is capable of producing small-scale, well-controlled explosions in a laboratory setting. The available diagnostic system in use provides valuable insight which enables better understanding of the physics of the interaction of cylindrical and spherical blast waves with structures.

The importance of experimentally validating numerical simulations was presented. Its ease of use and low operational costs together with the sophisticated diagnostics available facilitate accurate experimental results that can highlight the strengths and weaknesses of the numerical models for any specific problems of blast–structure interaction. After construction, calibration, and testing of the experimental system, various scenarios can be studied and numerical codes can be verified and validated.

To create three-dimensional blast waves, a small knot made from a copper wire was used. This setup created spherical blast waves that led to more realistic scenarios. The spherical nature of the exploding knot was tested and proved. The pressure histories recorded in a spherical blast experiment were compared to CONWEP generated results and found to be in good agreement.

Using dimensional analysis and similitude, experimental prediction of the load induced by the blast wave in this small-scale experimental setup can be used to assess the expected dynamic loads in the full-scale setup.

Acknowledgments The authors would like to thank Dr. A. L. Levin for his constructive remarks. This study is partially supported by the Israel Ministry of Defense grants numbers 4440507635 and 4440130927. O. Ram is supported by the Adams scholarship program of the Israeli Academy of Science.

References

Baker, W. (1973). *Explosions in air* (pp. 54–77). Austin: University of Texas Press.

Bennet, F. D. (1959). Flow fields produced by exploding wires. In W. G. Moore & H. K. Chace (Eds.), *Exploding wires proceedings* (Vol. 1, pp. 211–266). New York: Plenum Press.

Buntzen, R. R. (1962). The use of exploding wires in the study of small-scale underwater explosions. In W. G. Moore & H. K. Chace (Eds.), *Exploding wires proceedings* (Vol. 2, pp. 195–205). New York: Plenum Press.

Chase, W. G., & Moore, H. K. (1959). *Exploding wires*. New York: Plenum Press. 4 Volumes.

CONWEP. (1992). Conventional weapons effects, U. S. Army Engineer Waterways Experiment Station, CEWES-SS-R, 20 Aug 1992.

Cheval, K., Loiseau, O., & Vala, V. (2010). Laboratory scale tests for the assessment of solid explosive blast effects. Part I: Free-field test campaign. *Journal of Loss Prevention in the Process Industries, 23*(5), 613–621.

Dewey, J. M., McMillin, D. J., & Classen, D. F. (1977). Photogrammetry of spherical shocks reflected from real and ideal surfaces. *Journal of Fluid Mechanics, 81*, 701–717.

Dewey, J. M. (2001). Expending spherical shocks. In G. Ben-Dor, O. Igra, & T. Elperin (Eds.), *Handbook of shock waves* (Vol. 2, pp. 441–481). San Diego: Academic Press.

Hargather, J., & Settles, G. S. (2007). Optical measurement and scaling of blasts from gram-range explosive charges. *Shock Waves, 17*, 215–223.

Higashino, F., Henderson, L. F., & Shimizu, F. (1991). Experiments on the interaction of a pair of cylindrical weak blast waves in air. *Shock Waves, 1*, 275–284.

Jiang, Z., Takayama, K., Moosad, K. P. B., Onodera, O., & Sun, M. (1998). Numerical and experimental study of a micro-blast wave generated by pulsed-laser beam focusing. *Shock Waves, 8*, 337–349.

Kleine, H., & Takayama, K. (2004). Laboratory-scale blast wave phenomena. In B. Milton, T. Saito, & M. Sun (Eds.), *Proceedings of the symposium on Interdisciplinary Shock Wave Research* (pp. 257–276). Tohoku University.

Kleine, H., Timofeev, E., & Takayama, K. (2005). Laboratory-scale blast wave phenomena – Optical diagnostics and applications. *Shock Waves, 14*, 343–357.

Lin, S. C. (1954). Cylindrical shock waves produced by instantaneous energy release. *Journal of Applied Physics, 25*, 54–57.

Needham, C. E. (2010). *Blast waves*. Heidelberg: Springer.

Neuberger, A., Peles, S., & Rittel, D. (2007). Scaling the response of circular plates subjected to large and close-range spherical explosions. Part I: Air-blast loading. *International Journal of Impact Engineering, 34*, 859–873.

Ostraich, B., Kivity, Y., Anteby, I., Sadot, O., & Ben-Dor, G. (2009). Load assesment on safe rooms doors report. Shock Tube Laboratory, Protective Technologies R&D Center, Faculty of Engineering Sciences, Ben-Gurion University of the Negev, Beer-Sheva, Israel (in Hebrew).

Ram, O., & Sadot, O. (2012). Implementation of the exploding wire technique to study blast-wave–structure interaction. *Experiments in Fluids, 53*, 1335–1345. https://doi.org/10.1007/s00348-012-1339-8.

Reichenbach, H., & Neuwald, P. (2000). *Fluid-dynamics of explosions in multi-chamber systems phenomenology test program*. Freiburg: Ernst-Mach Institute.

Reithel, R. J., Blackburn, J. H., Seay, G. E., & Skolnick, S. (1962). The current pause in an exploding wire. In W. G. Moore & H. K. Chace (Eds.), *Exploding wires proceedings* (Vol. 1, pp. 19–32). New York: Plenum Press.

Rose, T. A., & Smith, P. D. (2002). Influence of the principal geometrical parameters of straight city streets on positive and negative phase blast wave impulses. *International Journal of Impact Engineering, 27*, 239–376.

Settles, G. S. (2001). *Schlieren and shadowgraph techniques: Visualizing phenomena in transparent media*. New York: Springer.

Smith, P. D., Mays, G. C., Rose, T. A., Teo, K. G., & Roberts, B. J. (1992). Small scale models of complex geometry for blast over pressure assessment. *International Journal of Impact Engineering, 12*, 345–360.

Smith, P. D., & Hetherington, J. G. (1994). *Blast and ballistic loading of structures* (pp. 145–223). Oxford: Butterworth-Heinemann.

Taylor, G. I. (1950). The formation of a blast wave by a very intense explosion. I. Theoretical discussion. *Proceedings of the Royal Society of London. Series A, Mathematical and Physical Sciences, 201*(1065), 159–174.

Zyskowski, A., Sochet, I., Mavrot, G., Bailly, P., & Renard, J. (2004). Study of the explosion process in a small scale experiment – Structural loading. *Journal of Loss Prevention, 17*, 291–299.